Research Square

Preprints are preliminary reports that have not undergone peer review.
They should not be considered conclusive, used to inform clinical practice,
or referenced by the media as validated information.

Genome wide analysis and stress responsive expression patterns of the bromodomain gene family in apple

Polina Kuzmitskaya

1401polina@gmail.com

National Academy of Sciences of Belarus

Alina Mazavets

National Academy of Sciences of Belarus

Oksana Urbanovich

National Academy of Sciences of Belarus

Research Article

Keywords: Apple (Malus × domestica), Bromodomain-containing proteins (MdBrD), Genome-wide identification, Transcription profile.

Posted Date: November 24th, 2026

DOI: https://doi.org/10.21203/rs.3.rs-11443702/v1

License: This work is licensed under a Creative Commons Attribution 4.0 International License.
Read Full License

Additional Declarations: No competing interests reported.

Polina Kuzmitskaya Alina Mazavets Oksana Urbanovich

Institute of Genetics and Cytology of the National Academy of Sciences of Belarus, Minsk, Belarus

E-mail address of the corresponding author: 1401polina@gmail.com, p.kuzmitskaya@igc.by

ORCID:

Polina Kuzmitskaya 0000-0002-1929-4315

Alina Mazavets 0009-0004-6523-8789

Oksana Urbanovich 0009-0008-7069-0891

Genome wide analysis and stress responsive expression patterns of the bromodomain gene family in apple

Abstract

Aim. This study performed a genome-wide *in silico* identification and a comprehensive bioinformatic analysis of the gene family encoding bromodomain-containing proteins (MdBrD) in apple (*Malus* × *domestica*).

Methods. Gene identification was conducted using HMMER3 and SMART software; the phylogenetic analysis and the evaluation of cis-regulatory elements were based on genomic sequencing data. Expression profiling was performed using transcriptomic data (RNA-seq) retrieved from the NCBI SRA databases for various tissues and stress conditions.

Results. Fifty *MdBrD* genes were identified in the apple genome distributed across 16 chromosomes and encoding 65 protein isoforms. The family is characterized by complex exon-intron organization (ranging from 1 to 23 exons) and high heterogeneity in domain architecture: in addition to the canonical bromodomain, modules such as SANT, PHD, WD40, helicase, and DNA-binding domains were identified. A high density of MYB, MYC, and WRKY binding sites, along with light- and phytohormone-responsive elements, was found in the promoter regions. Transcriptomic profiling confirmed pronounced tissue-specific expression (particularly during gametogenesis) and revealed a dose-dependent response to thermal and hypobaric stresses. Under biotic stress, a differential reaction to various pathogens was observed: *MdBrD* genes with antagonistic dynamics were identified, potentially reflecting the role of this family in switching between jasmonic and salicylic acid signaling pathways.

Keywords

Apple (*Malus* × *domestica*); Bromodomain-containing proteins (MdBrD); Genome-wide identification; Transcription profile.

Introduction

Plant resistance to abiotic stress is a complex, polygenically controlled trait. Both genetic and epigenetic components participate in the regulation of gene transcription. Post-translational modifications (PTMs) play a decisive role in defining the functional landscape of synthesized proteins, governing their catalytic efficiency and capacity for protein-protein interactions (Taunton et al. 1996). Among the diverse array of PTMs, acetylation, phosphorylation, and ubiquitination stand out as the most prominent examples (Kuo et al. 1996).

The dynamic interplay between histone acetylation and deacetylation is a fundamental mechanism for modulating chromatin architecture and regulating transcription factor access to DNA. The enzymatic machinery responsible for these changes — histone acetyltransferases and deacetylases — is often categorized as “writers” and “erasers” of the epigenetic code (Taunton et al. 1996; Kuo et al. 1996). Recognition of these marks is handled by “readers”, most notably bromodomains (first identified in the *Drosophila* Brahma protein) (Tamkun et al. 1992), as well as DPF and YEATS domains (e.g., Yaf9, ENL, AF9, Taf14, and Sas5) (Zeng et al. 2010; Li et al. 2014).

The bromodomain is a specialized protein module of approximately 110 residues characterized by a unique bundle of four α-helices (αZ, αA, αB, and αC). These helices are interconnected by two loops, ZA and BC, which together form a conserved hydrophobic pocket designed for the recognition of acetylated lysine on histone tails. A pivotal element for its binding capacity is a conserved asparagine residue located at the N-terminal part of the BC loop (Marmorstein and Berger 2001; Bottomley 2004; Mujtaba et al. 2007; Ferri et al. 2016). Within the cellular environment, BrDs function either independently or as part of larger multi-protein assemblies to modulate gene expression. Their primary role involves regulating chromatin accessibility through remodeling complexes that transition between condensed and decondensed states, thereby facilitating transcription factor binding (Florence and Faller 2001; Fujisawa and Filippakopoulos 2017). Among the ATP-dependent remodeling systems, the SWI/SNF complex is perhaps the most extensively documented. Its catalytic core, an ATPase known as BRAHMA (BRM), was first identified in yeast and subsequently in *Drosophila* (Tamkun et al. 1992). This complex promotes nucleosome sliding and disrupts histone-

DNA interactions via its SWI/SNF2-type ATPase subunit (Narlikar et al. 2002). Beyond simple recognition, BrDs play active roles in shaping the epigenetic landscape. One of their key functions is acting as enzymatic scaffolds that facilitate histone acetyltransferase (HAT) activity, thereby directly participating in the deposition of post-translational marks. Furthermore, many BrDs serve as molecular anchors, recruiting diverse transcriptional regulators to specific genomic loci enriched with acetylated histones. A classic illustration of this mechanism is found in the human BET protein family, which possesses both a bromodomain and an extra-terminal (ET) domain. These proteins utilize their bromodomains to tether themselves to acetylated chromatin, subsequently using the ET domain as a docking site for various transcriptional modulators (Rahman et al. 2011). Additionally, individual BrDs can operate as versatile transcriptional co-regulators. Depending on the molecular context and the specific complexes they associate with, these proteins can exert either activating or repressive effects on gene expression (Fujisawa and Filippakopoulos 2017).

Bromodomains rarely function in isolation; they are typically integrated into complex protein architectures alongside other functional modules. These may include catalytic units, such as histone acetyltransferase (HAT) domains, or additional epigenetic "readers" like Plant Homeodomain (PHD) fingers, which recognize distinct histone marks. Furthermore, the presence of multiple bromodomains within a single polypeptide chain is a common structural feature, allowing for multivalent interactions with chromatin (Filippakopoulos et al. 2012; Fujisawa and Filippakopoulos 2017).

Genes encoding bromodomains (*BrD* gene family) are organized into multigene families comprising several dozen members. This organization of *BrD* genes is characteristic of humans, animals, and plants. Different family members may be responsible for various developmental stages or types of stress. For instance, 46 *BrD* genes have been identified in the human genome, participating in numerous processes, including gene activation, cell growth and division, and carcinogenesis (Filippakopoulos et al. 2012; Cochran et al. 2019; Boyson et al. 2021).

In plants, *BrD*s are vital for regulating developmental milestones like flowering time (Farrona et al. 2011; Li et al. 2015), often through gibberellin signaling (Zhang et al. 2023) and floral patterning (Farrona et al. 2011; Wu et al. 2012; Zhao et al. 2015). They are also deeply involved in abiotic stress adaptation, including the abscisic acid (ABA) pathway (Han et al. 2012). Key ABA components, such as PP2Cs and SnRK2s, physically interact with bromodomains to modulate their phosphorylation status (Peirats-Llobet et al. 2016). Furthermore, bromodomains coordinate responses to phosphate starvation (Li et al. 2015), salinity (Nguyen et al. 2019), heat shock (Putnam and Jankowsky 2013), and drought (Hall and Matson 1999), partly through interactions with DNA-damage regulators like *MMS21* (Yuan et al. 2014). Notably, the proteasomal degradation of BRAHMA enhances boron tolerance in *Arabidopsis* by preventing DNA damage caused by histone hyperacetylation (Sakamoto et al. 2018).

Currently, information regarding this gene family in apple is lacking, although it may prove valuable for further research into deciphering their functional significance under various conditions, including stress responses.

Materials and Methods

Nucleotide and hypothetical protein sequences of apple (*Malus* × *domestica*, cv. *Golden Delicious*) genes were obtained from the Genome Database for Rosaceae (rosaceae.org), and chromosome sequences were retrieved from the NCBI GenBank database. The HMM model for the Myb/SANT-LIKE bromodomain (PF00439) was downloaded from the PFAM database (El-Gebali et al. 2018). This model was used to search for matches among hypothetical apple protein sequences using HMMER3 (hmmer.org). Identified potential matches were validated by scanning with SMART (https://smart.embl.de/smart/change_mode.cgi) (Letunic et al. 2020). Sequences containing a bromodomain were classified as apple bromodomain-containing proteins (*MdBrDs*). Gene sequence alignment was performed using the BLAST algorithm (Altschul et al. 1997). Sequence similarity was visualized using the Circoletto online service (https://bat.infspire.org/circoletto/) (Darzentas 2010), which is based on Circos (Krzywinski et al. 2009). Phylogenetic analysis of the BrD protein family was performed using the maximum likelihood (ML) method implemented in IQ-TREE (Trifinopoulos et al. 2016) via the Los Alamos Web Server (https://www.hiv.lanl.gov/content/sequence/IQTREE/iqtree.html). Multiple sequence alignment was previously executed using the COBALT algorithm (https://www.ncbi.nlm.nih.gov/tools/cobalt/re_cobalt.cgi) (Papadopoulos and Agarwala 2007). Amino acid substitution model LG (Le and Gascuel 2008) with FreeRate heterogeneity (+R4) (Soubrier et al. 2012) was selected as the best-fit evolutionary model (Kalyaanamoorthy et al. 2017). Branch support was assessed using the Ultrafast Bootstrap (UFBoot) approximation with 1,000 replicates (Hoang et al. 2018). Phylogenetic tree visualization was performed using the Interactive Tree of Life (iTOL) v. 7.6 web server (https://itol.embl.de/) (Letunic and Bork 2024). The exon-intron structure of the genes was generated using the Gene Structure Display Server v.2.0 (GSDS v.2.0) (https://gsds.gao-lab.org/) (Hu et al. 2014). To study gene regulatory elements, a 2000 bp DNA sequence upstream of the start codon was analyzed. *Cis*-regulatory elements were identified using the PlantCARE database (https://bio.tools/plantcare) (Lescot et al. 2002). For gene expression visualization,

transcript abundance was quantified from RNA-Seq raw reads using Salmon (v.1.10.0) with the quasi-mapping algorithm and automatic library type detection (-l A) (Patro et al. 2017). The CDS sequences of 65 *MdBrD* genes were used as a reference transcriptome for index construction. The raw sequencing data used in this study were retrieved from the NCBI Sequence Read Archive (SRA) database (https://www.ncbi.nlm.nih.gov/sra) (Leinonen et al., 2011). To stabilize variance, TPM (Transcripts Per Million) values were $\log_2(X+1)$ transformed. For better visualization of expression patterns across tissues, the data were row-normalized using a 0 to 1 scale. Heatmap construction and hierarchical clustering were subsequently performed in Python using the Pandas and Seaborn libraries (McKinney, 2010; Waskom, 2021). Clustering was executed using the Ward linkage method and Euclidean distance for both rows (genes) and columns (tissues/samples). The resulting dendrograms reflect the similarity in expression profiles between individual genes and biological samples. The complete list of analyzed samples, including their BioProject, treatment, and reference article, is provided in Table 1.

Table 1. Transcriptome data used for expression analyses.

Group / Treatment	Cultivar	Tissue	BioProject	Reference
10 apple tissues (pollen, anthers, filaments, young leaves, petals, styles, stigmas, sepals, ovaries, receptacles)	Golden Delicious	Pollen, anthers, filaments, young leaves, petals, styles, stigmas, sepals, ovaries, receptacles	PRJNA419119	(Pratas et al. 2018)
Sunburn	Honeycrisp	Fruit	PRJNA858858	(Waite et al. 2023)
Hypobaric conditions	Granny Smith	Fruit	PRJNA293208	(Cukrov et al. 2016)
Iron and phosphorus deficiencies	M9	Root	PRJNA505541	(Valentinuzzi et al. 2019)
Alternaria alternata infection	Starking Delicious	Leaf	PRJNA349086	(Zhu et al. 2017)
ASGV infection	Fuji	Apple plantlets	PRJNA233486	(Chen et al. 2014)

Results

In the apple genome, we identified 50 genes containing characteristic conserved domains. Evaluation of their chromosomal distribution revealed that most chromosomes (except for chromosome 8) harbor at least one such gene. The highest number (six) is located on chromosome 9, while chromosomes 10 and 11 contain five genes each; in contrast, chromosome 2 carries only a single gene. Overall, no clear correlation was observed between the chromosome length and the number of encoded *MdBrD* genes (Figure 1).

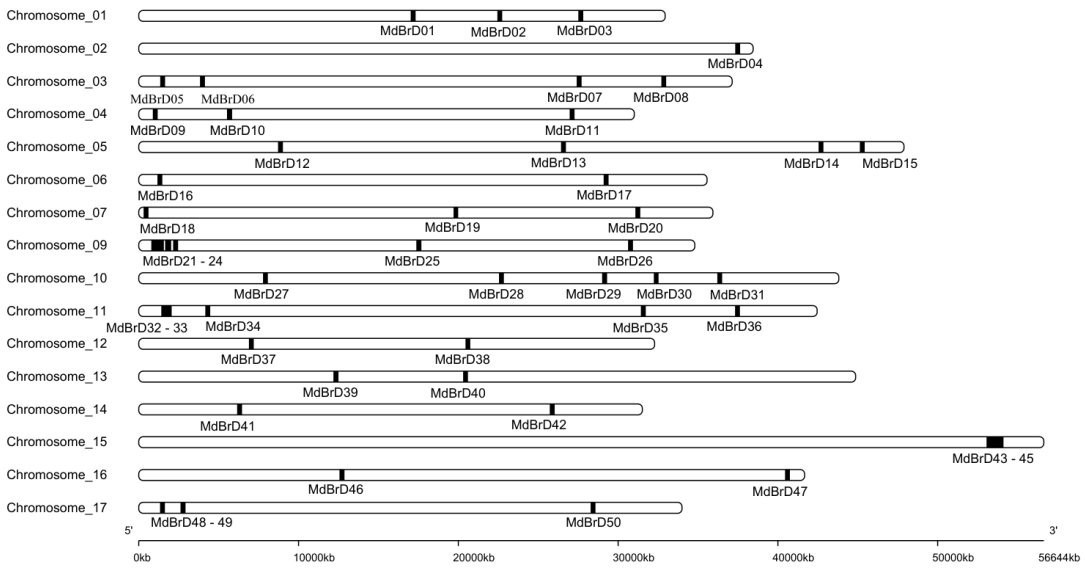

Figure 1. Chromosomal distribution of apple genes encoding bromodomain-containing proteins.

The phylogenetic relationship of the bromodomain-containing proteins is presented in Figure 2. As shown, the degree of their sequence identity does not depend on the chromosomal localization of their respective genes; those located on different chromosomes may encode more similar proteins than genes situated on the same chromosome. Notably, high similarity was observed among three gene pairs located on chromosomes 1 and 7, 9 and 17, and 13 and 16. This may serve as evidence of segmental or gene block duplications during the evolution of the apple genome.

The model for the origin of the *M. × domestica* genome, based on sequencing results, suggests that chromosome pairs 9 and 17, and 13 and 16 were derived from chromosomes III and IV of the ancestral species, respectively (Velasco et al. 2010). This explains the high degree of structural similarity between the gene pairs *MdBrD24–MdBrD49* and *MdBrD39–MdBrD46*. Chromosomes 1 and 7 also share a common origin; they are thought to have formed through duplications and subsequent chromosomal rearrangements of ancestral chromosomes VII and VIII (Velasco et al. 2010). The similarity between genes *MdBrD01* and *MdBrD18* is likely a result of these evolutionary events.

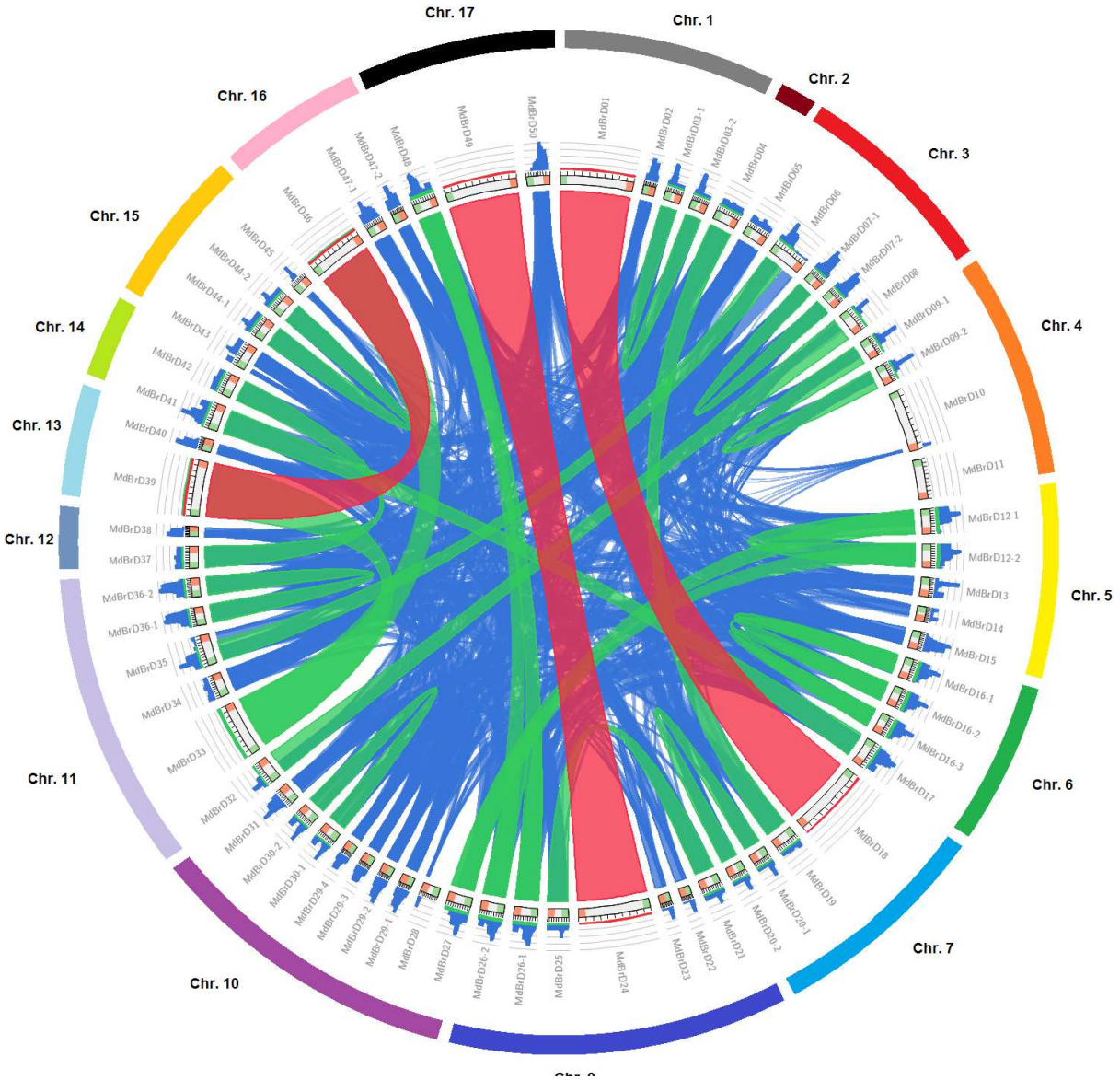

Figure 2. Phylogenetic relationships of apple MdBrD. Colored by score (min → max: blue → green → orange → red).

Analysis of the Gene Structure and Motifs in Apple Bromodomain-Containing Proteins

Apple bromodomain-containing proteins are encoded by genes characterized predominantly by a complex exon-intron organization (Figure 3A). The number of exons varies across genes, ranging from a single exon (in *MdBrD22* and *MdBrD23*) to 23 exons (*MdBrD33* and *MdBrD39*). Furthermore, a subset of these genes encodes multiple protein isoforms. For instance, *MdBrD29* encodes four isoforms, differing in their amino acid sequence length (designated as *MdBrD29-1* to *MdBrD29-4* in descending order of length, following the nomenclature used for all isoforms in this study). *MdBrD16* encodes three isoforms, while *MdBrD03*, *MdBrD07*, *MdBrD09*, *MdBrD12*, *MdBrD20*, *MdBrD26*, *MdBrD30*, *MdBrD36*, *MdBrD44*and *MdBrD47* each encode two isoforms. For the remaining genes, there is currently no evidence of multiple protein forms. Consequently, the 50 identified genes encode a total of 65 proteins, including all isoforms.

The majority of *MdBrD* proteins harbor consensus sequences of conserved amino acid motifs (Fig. 3B). Sequences with similar motif compositions group into clusters that correspond to the results of the phylogenetic analysis (Figs. 2 and 3). Motif 2 is most prevalent, occurring 63 times across the *MdBrD* sequences, including isoforms. Motif 1 is found 58 times, Motif 3 occurs 47 times, Motif 6 appears 37 times, and Motif 7 is detected 24 times. Motifs 4, 5, 8, 9, and 10 are less frequent, occurring 19, 17, 10, 12, and 7 times, respectively.

Figure 3C visualizes the domains identified within the *MdBrD* sequences using the SMART algorithm. According to these data, several proteins contain additional functional modules alongside the bromodomain. For example, *MdBrD33*, *MdBrD39*, and *MdBrD46*, which form a single cluster, contain a series of WD40 domains. The WD40 repeat (also known as the WD or beta-transducin repeat) is a short structural motif of approximately 40 amino acids, frequently terminating in a tryptophan-aspartic acid (WD) dipeptide. Tandem copies of these repeats typically fold together to form a circular solenoid structure known as the WD40 domain. WD40-repeat proteins constitute a large family found in all eukaryotes and are involved in diverse functions ranging from signal transduction and transcriptional regulation to cell cycle control, autophagy, and apoptosis. The primary shared function of all WD40-repeat proteins is the coordination of multi-protein complex assemblies, where the repeating units serve as a rigid scaffold for protein-protein interactions. The functional specificity of these proteins is determined by the sequences flanking the repeats themselves (Neer et al. 1994; Stirnimann et al. 2010; Jain and Pandey 2018).

The structurally similar *MdBrD01* and *MdBrD18* harbor four functional modules besides the bromodomain: QLQ, DEXDc, HELICc, and the AT-hook. The QLQ domain is characterized by conserved Gln-Leu-Gln residues. Along with these, specific aromatic, hydrophobic, and acidic amino acid residues (such as Phe, Trp, Tyr, Leu, and Glu) as well as a Pro residue are strictly conserved. These positions are crucial for the structural integrity of the QLQ domain, which mediates protein-protein interactions (Kim et al. 2003). The DEXDc domain contains an ATP-binding region and belongs to the DEAD-like helicase superfamily involved in ATP-dependent RNA or DNA unwinding and transcriptional regulation (Fuller-Pace 2006; Putnam and Jankowsky 2013). HELICc represents the C-terminal domain of the helicase superfamily. Based on the organization of characteristic motifs, helicases are classified into four major superfamilies; all possess the ability to unwind nucleic acid duplexes with distinct directional polarity, translocating along the strands and utilizing the energy of NTP hydrolysis (Hall and Matson 1999; Caruthers and McKay 2002). Finally, the AT-hook is a small DNA-binding motif with a strict preference for A/T-rich regions, frequently found in various chromatin-remodeling proteins, including high-mobility group (HMG) factors and plant-specific transcriptional regulators (Meijer et al. 1996; Reeves and Beckerbauer 2001).

The PHD finger and RING finger domains were identified within the sequences of *MdBrD24* and *MdBrD49*. The PHD finger domain was first discovered in the plant homeodomain, from which it derived its name. It is a zinc-finger-like motif, similar to the C4HC3 zinc finger, found in nuclear proteins believed to be involved in epigenetic and chromatin-mediated transcriptional regulation. The PHD finger domain functions as an epigenome reader, controlling gene expression through the molecular recruitment of multi-protein chromatin regulator complexes and transcription factors (Schindler et al. 1993; Sanchez and Zhou 2011). The RING finger (Really Interesting New Gene) is a zinc-finger-type motif containing a C3HC4 amino acid motif that binds two zinc ions. This protein domain typically spans 40–60 amino acid residues. Many RING finger-containing proteins play a key role in the ubiquitination pathway (Hanson et al. 1991; Lovering et al. 1993; Borden and Freemont 1996). Additionally, *MdBrD49* contains an FYRC domain—an FY-rich C-terminal motif frequently found in various chromatin-associated proteins. It consists of approximately 100 amino acid residues, exhibiting a high abundance of phenylalanine and tyrosine residues. The functions of this domain remain not fully understood (Doerks et al. 2002; García-Alai et al. 2010).

MdBrD04, *MdBrD05*, *MdBrD14*, *MdBrD19*, *MdBrD34*, *MdBrD37*, and *MdBrD42*, clustered together, contain a SANT domain in addition to the bromodomain. This domain is found in nuclear receptor co-repressors and subunits of many chromatin remodeling complexes. The name SANT is an acronym for “Swi3, Ada2, N-Cor, and TFIIIB”, and it belongs to the extended SANT/Myb family (Aasland et al. 1996; Boyer et al. 2004).

MdBrD21, *MdBrD25*, *MdBrD43*, *MdBrD44*, and *MdBrD45*, grouped in a single cluster, contain the AT-hook DNA-binding domain alongside the bromodomain.

MdBrD10 contains UBQ and ZnF_C2HC domains. The UBQ (ubiquitin) domain consists of 76 amino acid residues highly conserved in eukaryotes. Ubiquitin functions through its post-translational attachment (ubiquitination) to other proteins, where such modifications alter protein function, localization, or trafficking, or target the protein for degradation by the 26S proteasome (Glickman and Ciechanover 2002; Schnell and Hicke 2003; Mukhopadhyay and Riezman 2007). The ZnF_C2HC domain is a member of the zinc finger (ZnF) family, which comprises relatively small protein motifs containing multiple finger-like protrusions that make tandem contacts with target molecules. Some of these domains bind zinc or other metals, interacting with DNA, RNA, protein, and/or lipid substrates (Klug 1999; Matthews and Sunde 2002; Hall 2005).

In the *MdBrD11* sequence, an AAA domain (ATPases Associated with diverse cellular Activities) was identified. It is characteristic of an extensive group of protein families sharing a common conserved module of approximately 230 amino acid residues. This domain belongs to the AAA+ superfamily of ring-shaped P-loop NTPases, which exert their activity through energy-dependent remodeling or translocation of macromolecules (Frickey and Lupas 2004; Iyer et al. 2004).

Thus, the apple bromodomain-containing proteins represent a highly heterogeneous group. They differ in their exon-intron structure, conserved motif compositions, and sets of functional domains. At the same time, proteins with significant similarity are found among them. The domains identified within the *MdBrD* sequences suggest their involvement in a network of interactions with nucleic acids and transcriptional regulation processes.

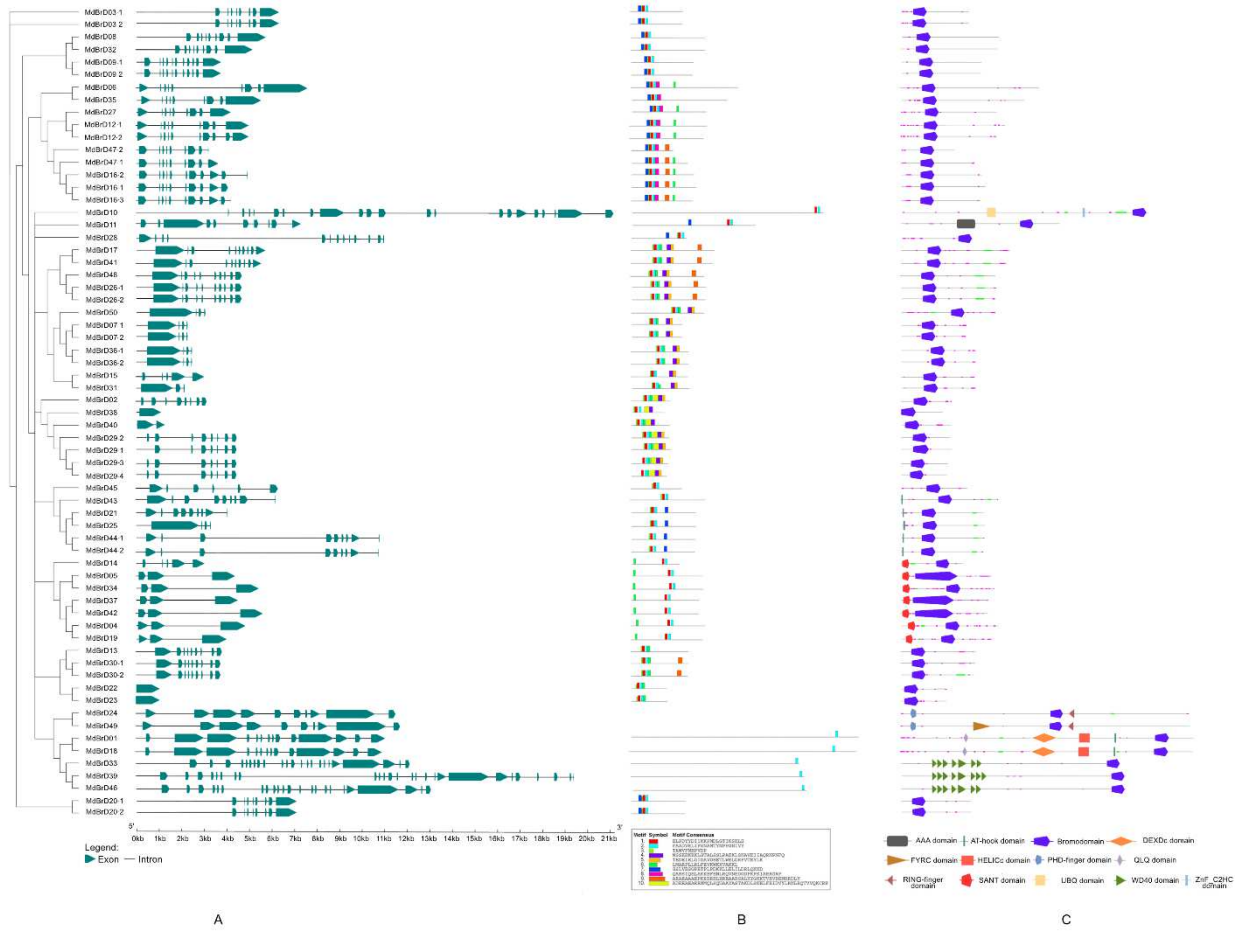

Figure 3. Structure of genes, amino acid motifs, and protein domains of apple bromodomain-containing proteins. (A) Phylogenetic relationships and gene structure; (B) Conserved motifs identified using the MEME algorithm; (C) Protein domains identified using the SMART algorithm.

The phylogenetic relationships of bromodomain-containing proteins from apple, rice, and *Arabidopsis* are presented in Figure 4. It demonstrates that BrDs constitute a heterogeneous group in which proteins from different genomes may exhibit greater similarity to each other compared to the proteins within the same genome.

The cluster assignment of proteins is often influenced by their domain composition. For example, the apple proteins MdBrD21, MdBrD25, MdBrD43, and MdBrD44, assigned to a single cluster, contain the AT-hook domain. Similarly, proteins containing a SANT domain in addition to the bromodomain are also grouped into a single cluster; this group includes the corresponding apple sequences alongside *Arabidopsis* and rice proteins (AT1G61215.1, AT2G42150.1, AT2G44430.1, AT3G60110.1, AT3G57980.1, and Os07G37800) that also possess this domain. The proteins MdBrD01 and MdBrD18, characterized by the presence of QLQ, DEXDc, HELICc, and AT-hook domains, were likewise assigned to the same cluster.

As shown by the data, the degree of sequence similarity between different species can exceed that found among proteins encoded within a single genome. This may serve as evidence of conserved similarity throughout evolution following speciation from a common ancestor, or as an example of convergent evolution at the protein level. In either case, it underscores the vital role of BrDs in the adaptation of various plant species to their environment. Conversely, some proteins show higher similarity to homologs within their own genome. These proteins may represent products of gene duplications that occurred within the respective plant genomes or copies resulting from whole-genome duplications.

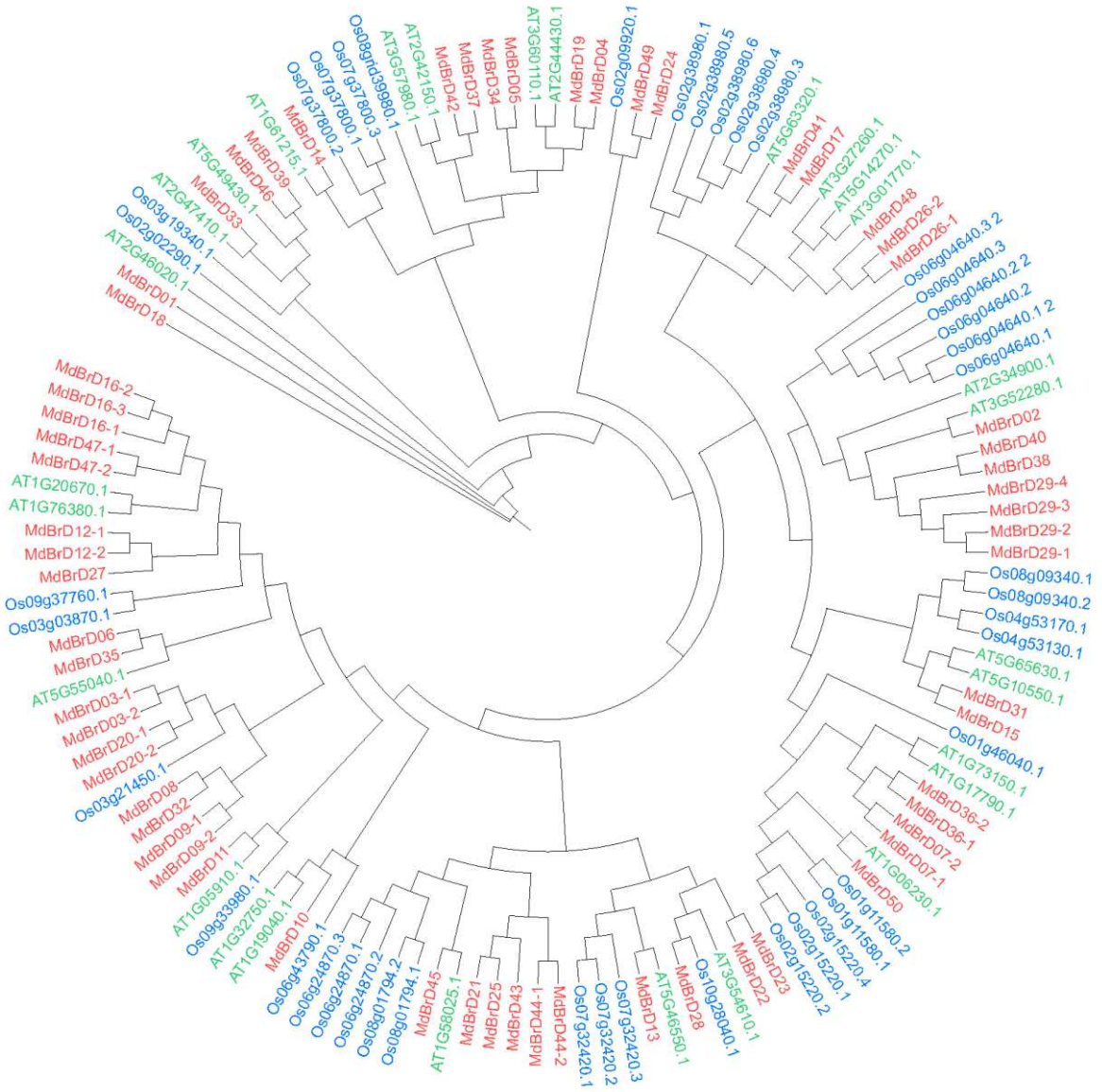

Figure 4. Phylogenetic relationships of bromodomain-containing proteins identified in the genomes of apple, rice, and *Arabidopsis thaliana* (shown in red, blue, and green, respectively).

Identification of putative cis-regulatory elements in the promoter regions of *MdBrD* genes

Analysis of the nucleotide structure of the regions upstream of the *MdBrD* genes indicates their involvement in a complex regulatory network governing vital physiological and developmental processes in plant cells.

Light is one of the key factors influencing the expression of *MdBrD* genes. Elements participating in light-dependent signaling pathways were identified in the promoter regions of all *MdBrD* family members without exception (Figure 5). Among these, the most prevalent are the G-box and Box 4, each identified in the promoter regions of 44 out of 50 genes (88%), followed by GT-1 (72%), GATA (50%), and the TCT-motif (46%). Other identified light-responsive elements include the 3-AF1 binding site, AAAC-motif, A-box, ACA-motif, ACE, AE-box, AT1-motif, ATC-motif, ATCT-motif, Box II, CAAT-box, CAG-motif, chs-CMA1a/2a, chs-Unit 1 m1, GA-motif, Gap-box, GTGGC-motif, I-box, LAMP-element, L-box, MRE, Sp1, TCC-motif, and TCCC-motif.

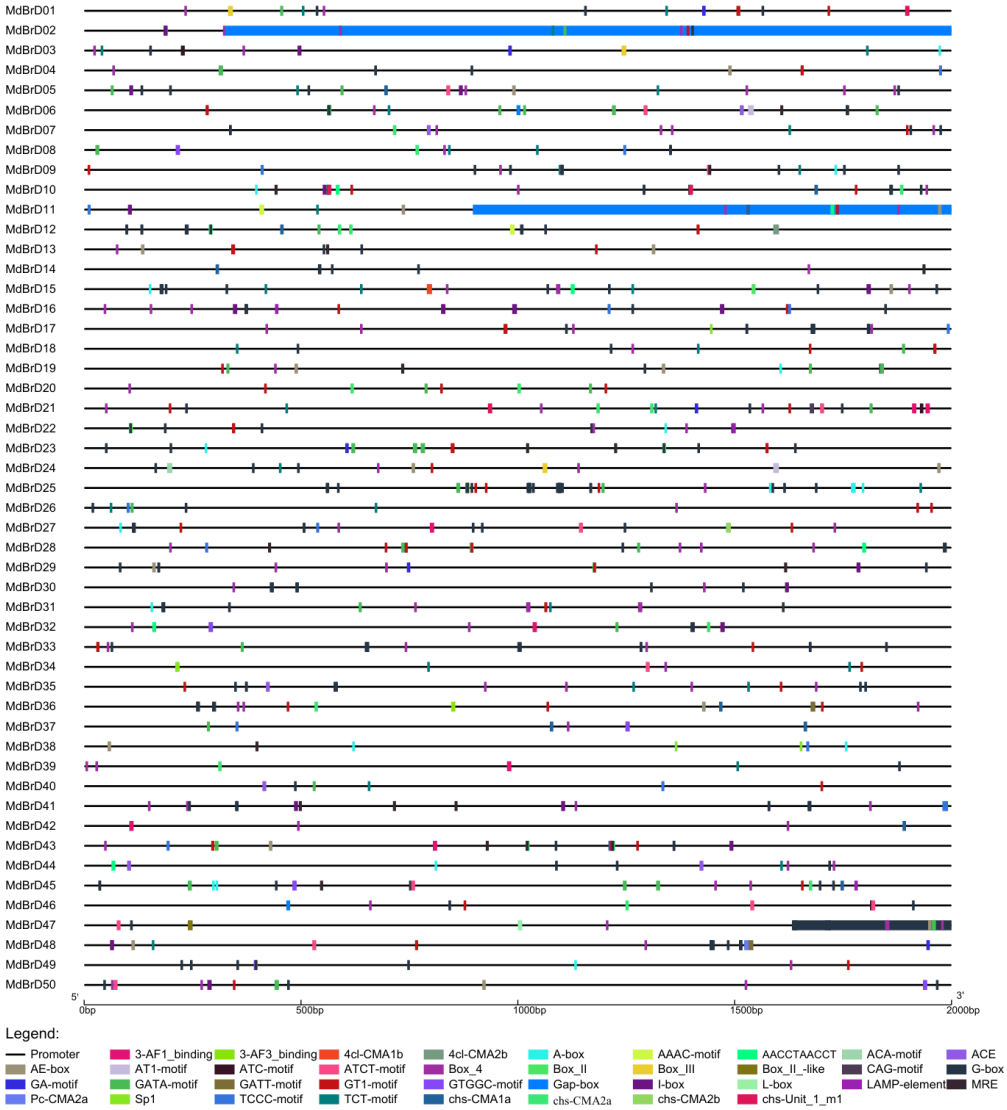

Figure 5. Binding sites for transcription factors involved in light-dependent signaling pathways identified in the promoter regions of *MdBrD* genes.

The expression of *MdBrD* genes under stress conditions is suggested by the presence of STRE elements (found in 84% of the promoter regions) and TC-rich repeats (40%). ARE elements, which participate in the anaerobic stress response, were identified in the regulatory regions of 43 genes (86%). One or more elements regulating gene expression during drought (MBS, DRE1, and DRE) were found in 64% of the promoters, while LTR elements, involved in the response to low-temperature exposure, were present in 54%. Potential *MdBrD* expression in response to wounding stress and pathogen attack is indicated by the presence of WUN, Box S, WRE3, and WRE motifs; at least one of them was found in the regulatory regions of 80% of the genes (Figure 6).

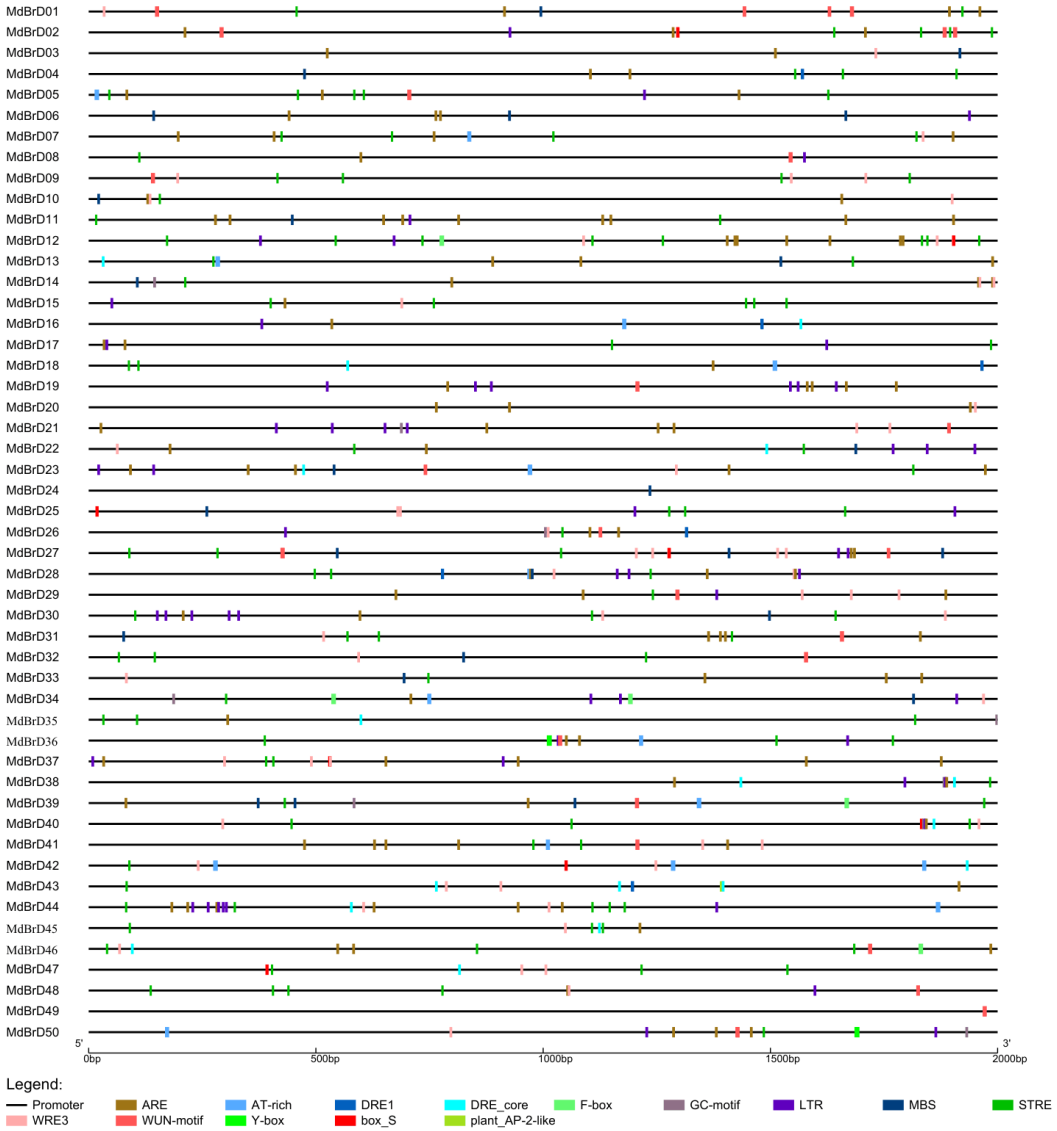

Figure 6. Binding sites for transcription factors involved in stress-induced signaling pathways identified in the promoter regions of *MdBrD* genes.

The induction of ***MdBrD* gene expression** can be triggered by plant hormones. Phytohormone-responsive elements were identified in the promoter regions of every gene, including those involved in response to abscisic acid (at least one ABRE, ABRE2, ABRE3a, ABRE4, or AT-ABRE element in 94% of the genes), gibberellin (at least one P-box, GARE, or CARE element in 46% of the promoters), salicylic acid (TCA and/or as-1 elements in 92% of the genes), and ethylene (ERE elements detected in 48% of cases). Additionally, CGTCA and/or TGACG sequences, which participate in the methyl jasmonate-induced signaling pathway, were found in the promoter regions of 78% of the genes. Various elements associated with hormone-regulated signaling cascades were identified in the promoter regions of every gene (Figure 7).

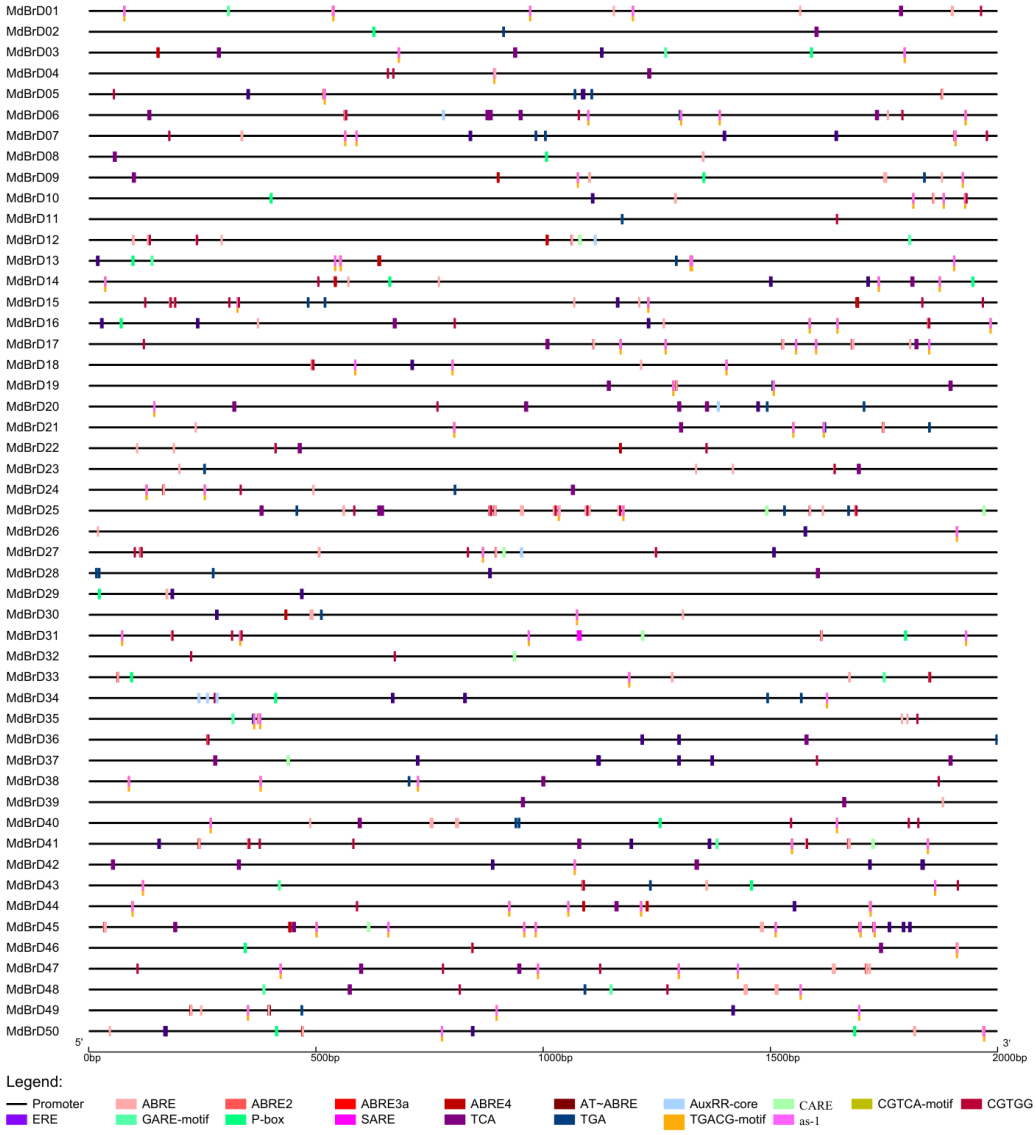

Figure 7. Binding sites for transcription factors involved in hormone-induced signaling pathways identified in the promoter regions of *MdBrD* genes.

Binding sites for regulatory proteins containing a MYB domain were identified in the promoter regions of every *MdBrD* gene. These proteins are involved in regulating responses to biotic and abiotic stress, including epigenetic control, hormonal signaling pathways, regulation of cell differentiation and shape, and phenylpropanoid biosynthesis. Notably, 98% of the *MdBrD* genes (with the exception of *MdBrD38*) contain characteristic DNA sequences for binding transcription factors from the MYC family. These factors are part of the jasmonic and salicylic acid hormonal regulation systems, participating in the coordination of plant growth and development, responses to various stressors, and other biological processes. Furthermore, 52% of the analyzed regulatory regions contain a W-box, a DNA sequence specifically recognized by WRKY transcription factors. WRKY factors perform numerous functions, including the mediation of disease and stress resistance, ontogenetic processes, and hormonal regulation.

The expression of individual *MdBrD* genes may be tissue-specific and dependent on the plant's developmental stage. This is evidenced by the presence of F-box elements (also involved in biotic and abiotic stress responses), O2-motifs (participating in prolamine metabolism), MBS-I sites (involved in flavonoid biosynthesis), and HD-Zip 1 binding sites (responsible for palisade mesophyll differentiation). The functional repertoire of *MdBrD* genes likely includes the regulation of proliferation and the cell cycle, as suggested by the identified regulatory elements rE2F-1, NON-box, and MSA-like.

In summary, analysis of the nucleotide structure of the regions immediately upstream of the *MdBrD* genes suggests their involvement in a complex network of regulatory processes essential for plant life. The identified regulatory

elements indicate that *MdBrD* expression occurs at distinct stages of ontogeny, while environmental conditions may lead to shifts in their transcription levels. This expression can be modulated by developmental stages, tissue and organ specificity, diverse environmental factors (including fluctuations in light intensity), and multiple types of biotic and abiotic stressors.

***MdBrD* gene family expression analysis**

To evaluate the tissue specificity of the *MdBrD* gene family, an expression analysis was conducted using transcriptomes from 10 different organs and tissues of the 'Golden Delicious' apple deposited in the NCBI Sequence Read Archive. The corresponding datasets were obtained from BioProject PRJNA419119 (Pratas et al. 2018). The results are visualized as a heatmap with hierarchical clustering where values range from 0.0 (minimum level, blue) to 1.0 (maximum level, red). The plot demonstrates that *MdBrD* genes exhibit pronounced tissue specificity (Figure 8). A characteristic feature of most investigated genes is an extremely low transcription level in pollen; however, a specific cluster of 14 genes shows high expression, which may indicate their involvement in male gametophyte development. In other floral organs, relatively high transcriptional activity is observed, suggesting the potential involvement of BrDs in flower formation and pollination mechanisms. Notably, the expression patterns of RNA isoforms generated via alternative splicing differ across all examined tissues.

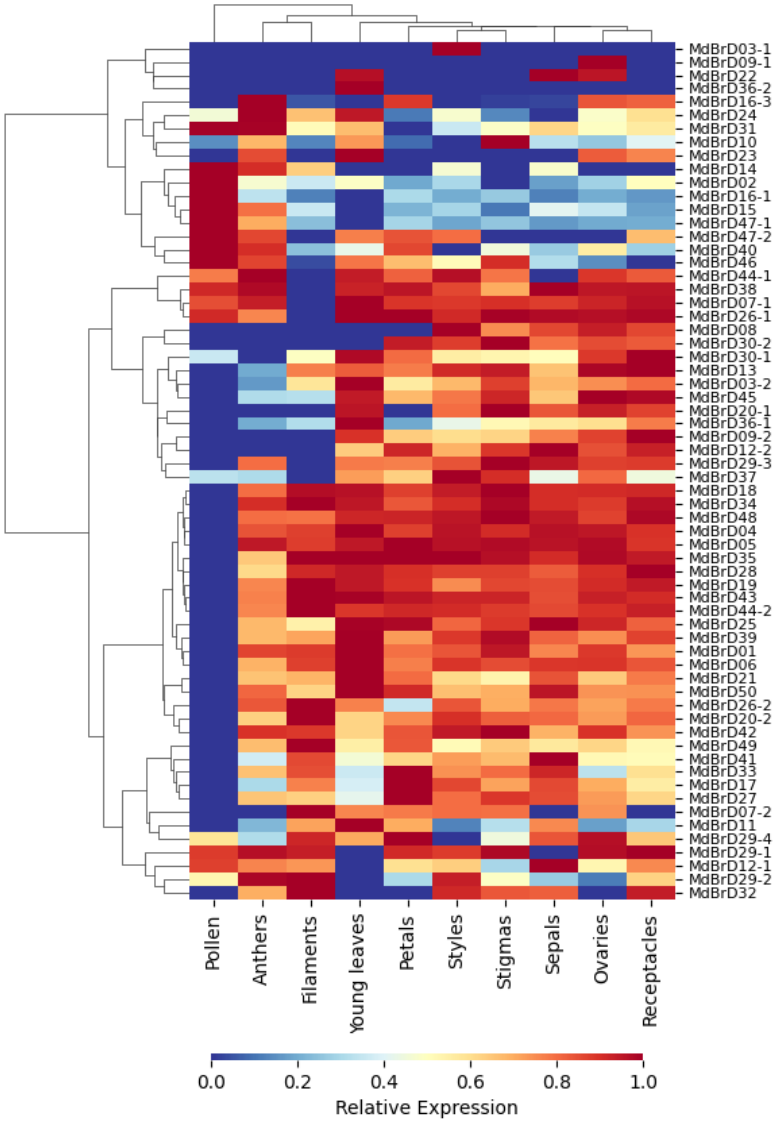

Figure 8. Heat map of *MdBrD* gene expression profiles in different tissues. RNA-seq relative expression data from 10 apple tissues (pollen, anthers, filaments, young leaves, petals, styles, stigmas, sepals, ovaries, receptacles) were used to reconstruct the expression patterns of *MdBrD* genes. The raw data were obtained from the NCBI Sequence Read Archive (PRJNA419119). To normalize the data and compress the range of expression values, raw TPM counts were $\log_2(X+1)$ transformed before clustering. Heat maps are presented in blue/yellow/red colors that represent

low/medium/high expression, respectively. On the left is a hierarchical clustering dendrogram reflecting the similarity of gene expression profiles.

To evaluate *MdBrD* expression under nutrient deficiency, we utilized raw data from Valentinuzzi et al. (2019) obtained from the NCBI Sequence Read Archive (PRJNA505541). This study employed root samples from apple rootstocks (*Malus* × *domestica*, Borkh., M9) subjected to iron and phosphorus deficiencies alongside a control group with normal nutrient supply. As shown in the heatmap in Figure 9, the deficiency of both nutrients caused a significant decrease in the expression of several *MdBrD* genes compared to the control (*MdBrD07* and *MdBrD36* for iron; *MdBrD36* and *MdBrD20* for phosphorus). Notably, the latter gene showed increased expression under iron deficiency. The multidirectional response of *MdBrD20* indicates functional specialization among individual family members. Furthermore, none of the genes showed more than a 3.5-fold increase in expression under nutrient deficiency compared to the control. The moderate nature of expression changes for most family members suggests that *MdBrD* genes are involved in modulating a physiological response rather than its primary induction.

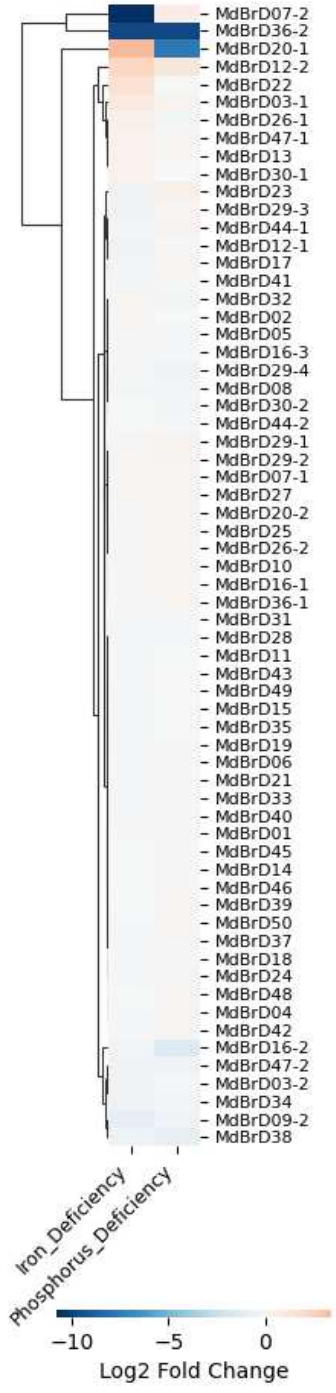

Figure 9. Heat map of *MdBrD* genes responses to iron and phosphorus deficiencies. RNA-seq relative expression data from apple roots were used to reconstruct the expression patterns of *MdBrD* genes. The raw data were obtained from the NCBI Sequence Read Archive (PRJNA505541). To stabilize variance, TPM values were $\log_2(X+1)$ transformed. Heat maps are presented in blue/white/red colors representing low/medium/high expression, respectively. On the left is a hierarchical clustering dendrogram reflecting the similarity of gene expression profiles.

To analyze the expression profiles of *MdBrDs* in response to the damaging effects of sunlight and high temperatures, data from BioProject PRJNA858858 were obtained from the NCBI Sequence Read Archive. In this experiment, 'Honeycrisp' apple fruits were subjected to control, below sunburn temperature (43–45°C), and above sunburn temperature (47–49°C) conditions, with samples collected 24, 48, and 72 h following the heat stimulus (Waite et al. 2023). The heatmap presented in Figure 10 shows that thermal exposure both above and below the sunburn threshold results in similar expression patterns for *MdBrD* genes; however, a more pronounced response is observed under more intensive exposure.

Four major clusters of *MdBrD* genes can be identified on the heatmap. The upper cluster brings together family members characterized by a decrease in expression levels after 24 hours of exposure compared to the control. The most dramatic drop in expression (reaching $\log_2$FC approx -10 and lower) was recorded at the 48-hour point for each treatment. Such a pattern indicates that these loci undergo stringent negative regulation in response to sunburn, leading to a significant depletion of their mRNA pool relative to the baseline (control) level.

The second gene cluster (central segment) includes the most numerous group of family members characterized by low sensitivity to the studied factors. The stability of their expression compared to the control over a wide time range (24–72 h) suggests that these *MdBrD* representatives are not involved in specific adaptive reactions to the investigated factors.

The third cluster consists of genes with a high response amplitude. This group demonstrates the most dynamic changes relative to control values. In contrast to the previous cluster, contrasting regulation is observed here. After 24 hours of exposure, a subset of genes shows a decrease in expression levels in both the above- and below-sunburn groups. However, after 48 hours, expression in the former group recovers to near-control levels, while in the latter, expression levels of most genes increase.

Finally, representatives of the fourth cluster demonstrate an increase in expression levels compared to the control 48 hours after exposure.

The analysis of *MdBrD* expression profiles revealed a heterogeneous response to thermal stress and light exposure (Fig. 10). The division of *MdBrD* genes into functional groups, ranging from stably expressed (Cluster 2) to those demonstrating sharp suppression (Cluster 1) or high dynamism (Clusters 3 and 4), indicates functional specialization of family members in adaptive responses of apple. A characteristic feature is the presence of a dose-dependent effect: a more intense stimulus (above sunburn temperature) induces more profound transcriptomic changes. The identification of genes with high response amplitudes and contrasting regulation suggests their potential as markers for thermal stress.

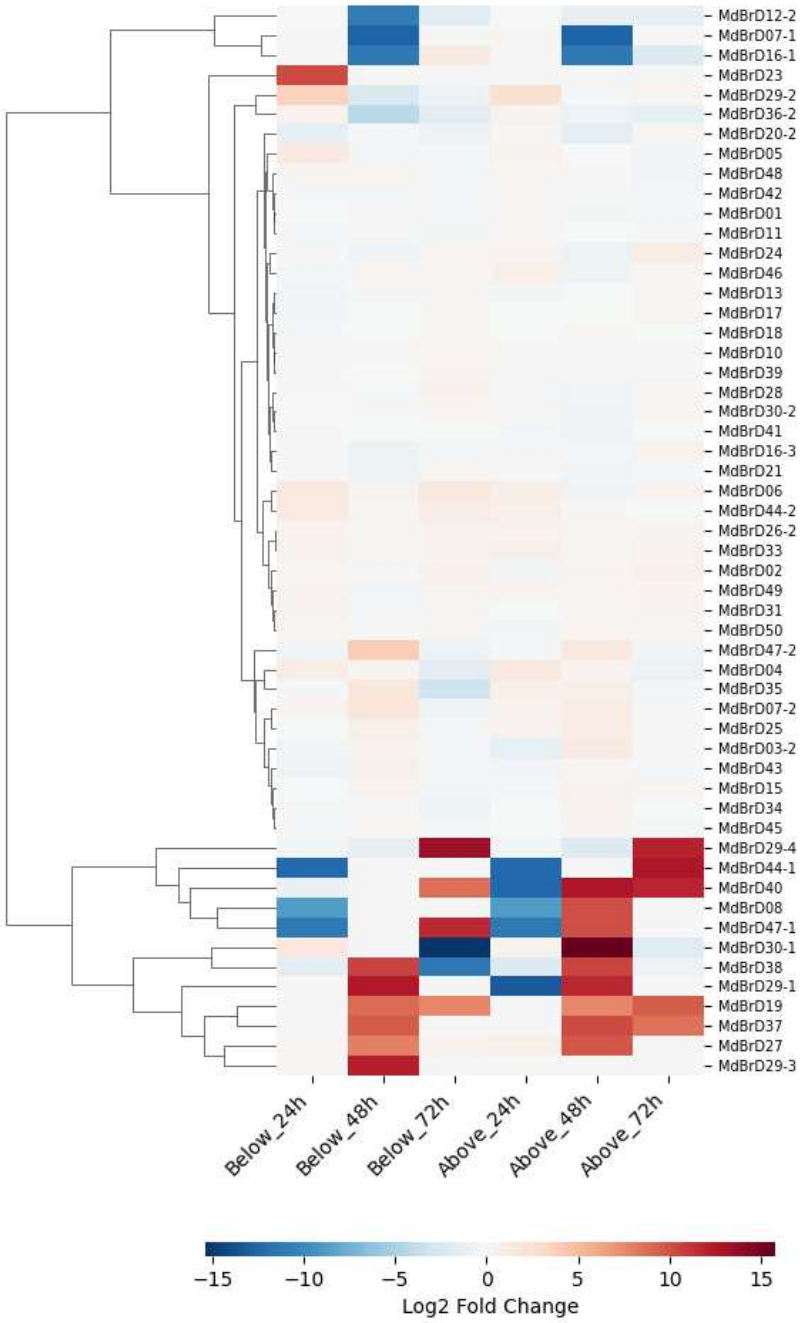

Figure 10. Heat map of *MdBrD* gene responses to sunburn conditions. RNA-seq relative expression data from apple peels were used to reconstruct the expression patterns of *MdBrD* genes. The raw data were obtained from the NCBI Sequence Read Archive (PRJNA858858). To stabilize variance, TPM values were $\log_2(X+1)$ transformed. Heat maps are presented in blue/white/red colors representing low, medium, and high expression, respectively. On the left is a hierarchical clustering dendrogram reflecting the similarity of gene expression profiles. "Below" and "above" indicate samples exposed to temperatures below the sunburn threshold (43–45 °C) and above the sunburn threshold (47–49 °C), respectively. 24, 48, and 72 h denote the time following the heat stimulus.

To evaluate the response of *MdBrD* genes to hypobaric stress, we utilized raw data from Cukrov et al. (2016) obtained from the NCBI Sequence Read Archive (PRJNA293208). In this experiment, apple fruits (*Malus domestica*, cv. Granny Smith) harvested at the commercial ripening stage were stored at 1 °C under normoxic (control) and hypoxic (0.4 and 0.8 kPa oxygen) conditions; RNA extraction was performed 24 days after hypoxic treatment. To assess *MdBrD* expression levels, a comparative analysis of their expression ($\log_2$ fold change) was conducted under two pressure regimes: 0.4 kPa and 0.8 kPa. Heatmap analysis (Fig. 11) revealed that the majority of the investigated genes exhibited weak or moderate sensitivity to pressure changes. Nevertheless, a group of genes with a pronounced change in transcript levels was identified. The strongest positive response at a pressure of 0.4 kPa was demonstrated by the *MdBrD36-2* isoform. Conversely, isoforms *MdBrD20-1* and *MdBrD29-3* showed a significant decrease in expression levels at 0.4 kPa. Under 0.8 kPa conditions, changes in expression levels were less substantial. Response patterns of

these *MdBrD* family members to hypobaria indicate their functional diversification and the dose-dependent nature of expression for specific representatives.

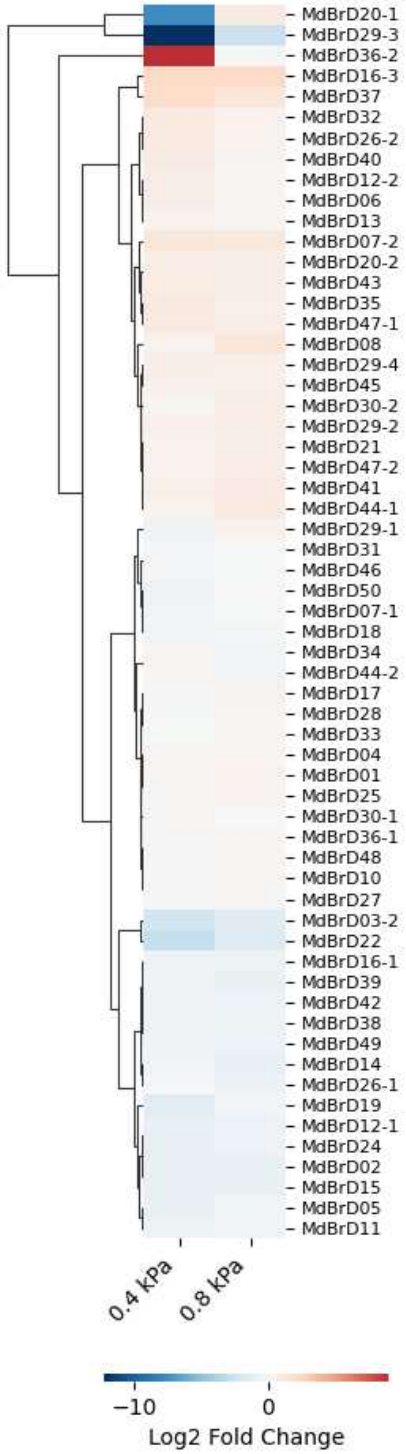

Figure 11. Heat map of *MdBrD* gene responses to hypobaric conditions. RNA-seq data from apple fruit tissues were used to reconstruct the expression patterns of *MdBrD* genes. The raw data were obtained from the NCBI Sequence Read Archive (PRJNA293208). To stabilize variance, TPM values were $\log_2$-transformed ($\log_2(X+1)$). The heatmap is presented in a blue-white-red color scale, corresponding to low, medium, and high expression levels, respectively. On the left is a hierarchical clustering dendrogram reflecting the similarity of gene expression profiles. The labels "0.4 kPa" and "0.8 kPa" correspond to samples subjected to different pressure regimes.

The impact of biotic stress (pathogen attack) was evaluated using the examples of infection by the fungus *Alternaria alternata* Apple Pathotype and Apple stem grooving virus (ASGV). Raw sequence data from 'Starking Delicious' apple leaves at 12, 18, 36, and 72 hours post-infection were obtained from the NCBI Sequence Read Archive (PRJNA349086) (Zhu et al. 2017). Raw data from in vitro-grown ASGV-infected and virus-free plantlets of apple cv.

Fuji were obtained from the NCBI Sequence Read Archive (PRJNA233486) (Chen et al. 2014). Comparative analysis revealed that *MdBrD* family genes respond differentially to a necrotrophic fungal infection by *A. alternata* and a systemic viral infection by ASGV. The heatmaps are presented in Fig. 12A (*Alternaria alternata* Apple Pathotype infection) and Fig. 12B (ASGV).

The *A. alternata* infection induced a significant activation of a specific group of genes and alternative transcripts (*MdBrD20-1*, *MdBrD29-1*, *MdBrD36-2*, and *MdBrD47-2*) during the 12–18 hour post-infection interval. For the *MdBrD22* gene, an increased expression level was observed 36 hours after infection. Expression levels of *MdBrD07-2*, *MdBrD12-2*, *MdBrD08*, and *MdBrD29-3* decreased. Specifically, *MdBrD07-2* expression declined relative to the control over time, reaching its minimum by 72 hours, whereas the expression levels of other genes showed minimal differences from the control by the 72-hour mark of the infection.

ASGV-infected apple trees demonstrated decreased expression levels of *MdBrD22* and *MdBrD30-2* compared to the control and increased levels of *MdBrD07-2*, *MdBrD29-1*, *MdBrD08*, and *MdBrD23*.

The response of *MdBrD* family genes to pathogens is highly specific. Genes activated during fungal infection *(A. alternata)* may be suppressed during viral infection (ASGV) and vice versa. Prominent examples are *MdBrD07-2* and *MdBrD08*, whose expression drops during fungal infection but rises in the presence of the virus. The *MdBrD29-1* transcript acts as a universal positive responder to both types of stress, increasing expression under both fungal and viral infection. In contrast, the *MdBrD22* gene demonstrates multidirectional dynamics. These differences in gene response may be explained by the fact that plants utilize fundamentally different signaling pathways and defense mechanisms to combat fungi and viruses. Fungal infection typically triggers the jasmonic acid pathway, which facilitates defense against necrotrophic pathogens, herbivores, and induced systemic resistance. In contrast, salicylic acid plays a key role in defending against biotrophic pathogens, including viruses, promoting local and systemic acquired resistance. These signaling pathways are often antagonistic, and the activation of one frequently requires the suppression of the other (Zhang et al. 2025).

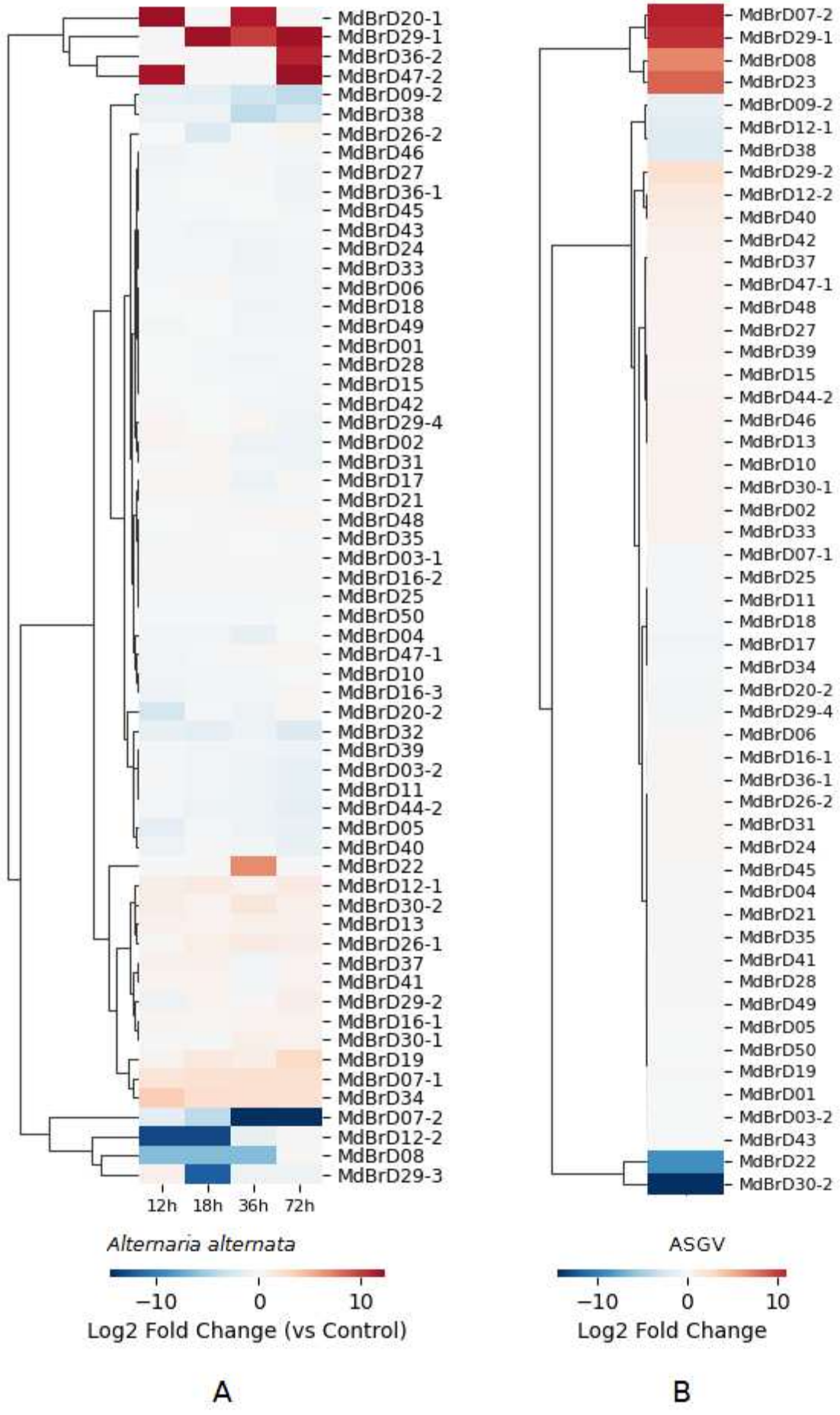
MdBrD20-1
MdBrD29-1
MdBrD36-2
MdBrD47-2
MdBrD09-2
MdBrD38
MdBrD26-2
MdBrD46
MdBrD27
MdBrD36-1
MdBrD45
MdBrD43
MdBrD24
MdBrD33
MdBrD06
MdBrD18
MdBrD49
MdBrD01
MdBrD28
MdBrD15
MdBrD42
MdBrD29-4
MdBrD02
MdBrD31
MdBrD17
MdBrD21
MdBrD48
MdBrD35
MdBrD03-1
MdBrD16-2
MdBrD25
MdBrD50
MdBrD04
MdBrD47-1
MdBrD10
MdBrD16-3
MdBrD20-2
MdBrD32
MdBrD39
MdBrD03-2
MdBrD11
MdBrD44-2
MdBrD05
MdBrD40
MdBrD22
MdBrD12-1
MdBrD30-2
MdBrD13
MdBrD26-1
MdBrD37
MdBrD41
MdBrD29-2
MdBrD16-1
MdBrD30-1
MdBrD19
MdBrD07-1
MdBrD34
MdBrD07-2
MdBrD12-2
MdBrD08
MdBrD29-3
12h
18h
36h
72h
Alternaria alternata
−10
0
10
Log2 Fold Change (vs Control)
A
MdBrD07-2
MdBrD29-1
MdBrD08
MdBrD23
MdBrD09-2
MdBrD12-1
MdBrD38
MdBrD29-2
MdBrD12-2
MdBrD40
MdBrD42
MdBrD37
MdBrD47-1
MdBrD48
MdBrD27
MdBrD39
MdBrD15
MdBrD44-2
MdBrD46
MdBrD13
MdBrD10
MdBrD30-1
MdBrD02
MdBrD33
MdBrD07-1
MdBrD25
MdBrD11
MdBrD18
MdBrD17
MdBrD34
MdBrD20-2
MdBrD29-4
MdBrD06
MdBrD16-1
MdBrD36-1
MdBrD26-2
MdBrD31
MdBrD24
MdBrD45
MdBrD04
MdBrD21
MdBrD35
MdBrD41
MdBrD28
MdBrD49
MdBrD05
MdBrD50
MdBrD19
MdBrD01
MdBrD03-2
MdBrD43
MdBrD22
MdBrD30-2
ASGV
−10
0
10
Log2 Fold Change
B

Figure 12. Heat map of *MdBrD* gene responses to biotic stress. RNA-seq data from apple leaves (for the *Alternaria alternata* infection) and apple plantlets (for the ASGV infection) were used to reconstruct the expression patterns of *MdBrD* genes. The raw data were obtained from the NCBI Sequence Read Archive (PRJNA349086 and PRJNA233486, respectively). To stabilize variance, TPM values were $\log_2$-transformed ($\log_2(X+1)$). The heatmap is presented in a blue-white-red color scale corresponding to low, medium, and high expression levels, respectively. On the left is a hierarchical clustering dendrogram reflecting the similarity of gene expression profiles. The labels "12h", "18h", "36h", and "72h" (Panel A) indicate the time post-infection with the fungus *Alternaria alternata*; the label "ASGV" (Panel B) corresponds to the samples infected with the Apple stem grooving virus.

Conclusion

The identification of 50 *MdBrD* genes distributed across 16 chromosomes and their phylogenetic analysis demonstrated that their evolutionary relationships are consistent with the origin of the apple genome. The high variability of the exon-intron structure and the presence of 65 protein isoforms indicate significant post-transcriptional regulation and functional diversification within the *MdBrD* family. The discovery of additional regulatory modules within MdBrDs (SANT, PHD, WD40, AAA-ATPases, helicase domains, and zinc fingers) suggests that these proteins participate not only in histone code reading but also in active chromatin remodeling, ATP-dependent macromolecule translocation, and ubiquitination processes.

Transcriptomic profiling revealed a pronounced specialization in *MdBrD* gene expression. The presence of cell cycle control elements (rE2F-1, MSA-like) in the promoters confirms the involvement of this family in fundamental processes of tissue proliferation and differentiation. *MdBrD* genes were shown to be integrated into response systems for nutrient, thermal, and hypobaric stresses. The expression patterns are dose-dependent, ranging from moderate modulation during iron and phosphorus deficiencies to the profound suppression ($\log_2$FC less than or equal to -10) or the sharp induction of specific isoforms during thermal shock and hypoxia, allowing them to be considered potential markers for stress tolerance.

The family's response to biotic stress is pathogen-specific. The multidirectional expression dynamics of key loci during *A. alternata* and ASGV infection may indicate the role of MdBrDs in coordinating antagonistic salicylic and jasmonic acid signaling pathways. Thus, *MdBrD* genes serve as multifunctional regulators ensuring the plasticity of the apple's physiological response by integrating external stimuli with internal genetic developmental programs. These findings supplement existing knowledge about genome regulation mechanisms in woody crops and provide a basis for identifying molecular markers useful in apple breeding for stress resistance.

Funding

This research was funded by the National Academy of Sciences of Belarus, task number 2.10.6.

Declarations

A. Acknowledgments

The authors are deeply grateful to the researchers for depositing the respective SRA archives under BioProjects PRJNA419119, PRJNA858858, PRJNA293208, PRJNA505541, PRJNA349086, and PRJNA233486 in the NCBI SRA public database, making this analysis possible. The authors highly appreciate their contribution to the advancement of Open Science principles.

B. Author contributions

P. K. and O. U. conceived and designed the study. P. K. and A. M. performed the bioinformatic analysis and analyzed the data. P. K. wrote the main manuscript text and prepared figures 4-12. A. M. prepared figures 1-3. All authors reviewed the manuscript.

C. Clinical trial number

Not applicable.

D. Consent to participate

Not applicable.

E. Consent to publish

Not applicable. This study involved exclusively the bioinformatic re-analysis of publicly available genomic and transcriptomic datasets retrieved from the Genome Database for Rosaceae (GDR) and NCBI GenBank/SRA. No live plant materials were collected, cultivated, or sampled by the authors for this study, and no field experiments were conducted. Therefore, specific plant collection guidelines, permissions, or licenses were not required.

F. Conflicts of interest

The authors declare no conflict of interest.

G. Ethical approval

Not applicable.

H. Data availability statements

The data supporting the findings of this study were derived from publicly available repositories. Apple (Malus × domestica) genomic and protein sequences are available in the Genome Database for Rosaceae (rosaceae.org) and the NCBI GenBank database. Raw RNA sequencing datasets analyzed during this study were retrieved from the NCBI Sequence Read Archive (SRA) database (https://www.ncbi.nlm.nih.gov/sra) under BioProject accession numbers PRJNA419119, PRJNA858858, PRJNA293208, PRJNA505541, PRJNA349086, and PRJNA233486. The HMM profile used for identification is available in the PFAM database. All software tools, databases, and web servers used for bioinformatic processing are publicly accessible via their final repository links: HMMER3 (hmmer.org), SMART (https://smart.embl.de/smart/change_mode.cgi), Circoletto (https://bat.infspire.org/circoletto/), IQ-TREE via the Los Alamos Web Server (https://www.hiv.lanl.gov/content/sequence/IQTREE/iqtree.html), NCBI COBALT (https://www.ncbi.nlm.nih.gov/tools/cobalt/re_cobalt.cgi), iTOL v. 7.6 (https://itol.embl.de/), GSDS v.2.0 (https://gsds.gao-lab.org/), and PlantCARE (https://bio.tools/plantcare). Python data analysis libraries used for visualization are accessible via Pandas and Seaborn. All newly analyzed data and analyzed datasets generated during the current study are included in this article.

References

Aasland R, Stewart AF, Gibson T (1996) The SANT domain: a putative DNA-binding domain in the SWI-SNF and ADA complexes, the transcriptional co-repressor N-CoR and TFIIIB. Trends Biochem Sci 21:87–88. doi.org

Altschul SF, et al (1997) Gapped BLAST and PSI-BLAST: a new generation of protein database search programs. Nucleic Acids Res 25:3389–3402. doi.org

Borden KLB, Freemont PS (1996) The RING finger domain: a recent example of a sequence—structure family. CurrOpin Struct Biol 6:395–401. doi.org

Bottomley MJ (2004) Structures of protein domains that create or recognize histone modifications. EMBO Rep 5:464–469. doi.org

Boyer LA, Latek RR, Peterson CL (2004) The SANT domain: a unique histone-tail-binding module? Nat Rev Mol Cell Biol 5:158–163. doi.org

Boyson SP, et al (2021) Functional Roles of Bromodomain Proteins in Cancer. Cancers (Basel) 13:3473. doi.org

Caruthers JM, McKay DB (2002) Helicase structure and mechanism. CurrOpin Struct Biol 12:123–133. doi.org

Chen S, et al (2014) Infection of apple by apple stem grooving virus leads to extensive alterations in gene expression patterns but no disease symptoms. PLoS One 9:e95239. doi.org

Cochran AG, Conery AR, Sims RJ (2019) Bromodomains: a new target class for drug development. Nat Rev Drug Discov 18:609–628. doi.org

Cukrov D, et al (2016) Extreme Hypoxic Conditions Induce Selective Molecular Responses and Metabolic Reset in Detached Apple Fruit. Front Plant Sci 7:146. doi.org

Darzentas N (2010) Circoletto: visualizing sequence similarity with Circos. Bioinformatics 26:2620–2621. doi.org

Doerks T, et al (2002) Systematic identification of novel protein domain families associated with nuclear functions. Genome Res 12:47–56. doi.org

El-Gebali S, et al (2018) The Pfam protein families database in 2019. Nucleic Acids Res 47:D427–D432. doi.org

Farrona S, et al (2011) Brahma is required for proper expression of the floral repressor FLC in Arabidopsis. PLoS One 6:e17997. doi.org

Ferri E, Petosa C, McKenna CE (2016) Bromodomains: Structure, function and pharmacology of inhibition. BiochemPharmacol 106:1–18. doi.org

Filippakopoulos P, et al (2012) Histone recognition and large-scale structural analysis of the human bromodomain family. Cell 149:214–231. doi.org

Florence B, Faller DV (2001) You bet-cha: a novel family of transcriptional regulators. Front Biosci6:D1008–D1018. doi.org

Frickey T, Lupas AN (2004) Phylogenetic analysis of AAA proteins. J Struct Biol 146:2–10. doi.org

Fujisawa T, Filippakopoulos P (2017) Functions of bromodomain-containing proteins and their roles in homeostasis and cancer. Nat Rev Mol Cell Biol 18:246–262. doi.org

Fuller-Pace FV (2006) DExD/H box RNA helicases: multifunctional proteins with important roles in transcriptional regulation. Nucleic Acids Res 34:4206–4215. doi.org

García-Alai MM, et al (2010) The structure of the FYR domain of transforming growth factor beta regulator 1. Protein Sci 19:1432–1438. doi.org

Glickman H, Ciechanover A (2002) The ubiquitin-proteasome proteolytic pathway: destruction for the sake of construction. Physiol Rev 82:373–428. doi.org

Hall MC, Matson SW (1999) Helicase motifs: the engine that powers DNA unwinding. Mol Microbiol 34:867–877. doi.org

Hall TM (2005) Multiple modes of RNA recognition by zinc finger proteins. CurrOpin Struct Biol 15:367–373. doi.org

Han SK, et al (2012) The SWI2/SNF2 Chromatin Remodeling ATPase BRAHMA Represses Abscisic Acid Responses in the Absence of the Stress Stimulus in Arabidopsis. Plant Cell 24:4892–4906. doi.org

Hanson IM, Poustka A, Trowsdale J (1991) New genes in the class II region of the human major histocompatibility complex. Genomics 10:417–424. doi.org

Hoang DT, Chernomor O, von Haeseler A, Minh BQ, Vinh LS (2018) UFBoot2: Improving the Ultrafast Bootstrap Approximation. Molecular Biology and Evolution 35 (2):518-522. doi:10.1093/molbev/msx281

Hu B, et al (2014) GSDS 2.0: an upgraded gene feature visualization server. Bioinformatics 31:1296–1297. doi.org

Iyer LM, et al (2004) Evolutionary history and higher order classification of AAA+ ATPases. J Struct Biol 146:11–31. doi.org

Jain BP, Pandey S (2018) WD40 Repeat Proteins: Signalling Scaffold with Diverse Functions. Protein J 37:391–406. doi.org

Kalyaanamoorthy S, Minh BQ, Wong TKF, von Haeseler A, Jermiin LS (2017) ModelFinder: fast model selection for accurate phylogenetic estimates. Nature Methods 14 (6):587-589. doi:10.1038/nmeth.4285

Kim JH, Choi D, Kende H (2003) The AtGRF family of putative transcription factors is involved in leaf and cotyledon growth in Arabidopsis. Plant J 36:94–104. doi.org

Klug A (1999) Zinc finger peptides for the regulation of gene expression. J Mol Biol 293:215–218. doi.org

Krzywinski MI, et al (2009) Circos: An information aesthetic for comparative genomics. Genome Res 19:1639–1645. doi.org

Kuo MH, et al (1996) Transcription-linked acetylation by Gcn5p of histones H3 and H4 at specific lysines. Nature 383:269–272. doi.org

Leinonen R, Sugawara H, Shumway M (2011) The sequence read archive. Nucleic Acids Res 39 (Database issue): D19-21. doi:10.1093/nar/gkq1019

Lescot M, et al (2002) PlantCARE, a database of plant cis-acting regulatory elements and a portal to tools for in silico analysis of promoter sequences. Nucleic Acids Res 30:325–327. doi.org

Letunic I, Khedkar S, Bork P (2020) SMART: recent updates, new developments and status in 2021. Nucleic Acids Res 49:D458–D460. doi.org

Letunic I, Bork P (2024) Interactive Tree of Life (iTOL) v6: recent updates to the phylogenetic tree display and annotation tool. Nucleic Acids Res 52 (W1):W78-W82. doi:10.1093/nar/gkae268

Li C, et al (2015) The Arabidopsis SWI2/SNF2 chromatin remodeler BRAHMA regulates polycomb function during vegetative development and directly activates the flowering repressor gene SVP. PLoS Genet 11:e1004944. doi.org

Li Y, et al (2014) AF9 YEATS domain links histone acetylation to DOT1L-mediated H3K79 methylation. Cell 159:558–571. doi.org

Lovering R, et al (1993) Identification and preliminary characterization of a protein motif related to the zinc finger. Proc Natl Acad Sci USA 90:2112–2116. doi.org

Marmorstein R, Berger SL (2001) Structure and function of bromodomains in chromatin-regulating complexes. Gene 272:1–9. doi.org

McKinney W (2010) Data Structures for Statistical Computing in Python. In: Proceedings of the 9th Python in Science Conference, pp 56–61. doi.org

Meijer AH, van Dijk EL, Hoge JH (1996) Novel members of a family of AT hook-containing DNA-binding proteins from rice are identified through their in vitro interaction with consensus target sites of plant and animal homeodomain proteins. Plant Mol Biol 31:607–618. doi.org

Mujtaba S, Zeng L, Zhou MM (2007) Structure and acetyl-lysine recognition of the bromodomain. Oncogene 26:5521–5527. doi.org

Mukhopadhyay D, Hiezman H (2007) Proteasome-independent functions of ubiquitin in endocytosis and signaling. Science 315:201–205. doi.org

Narlikar GJ, Fan HY, Kingston RE (2002) Cooperation between complexes that regulate chromatin structure and transcription. Cell 108:475–487. doi.org

Neer EJ, et al (1994) The ancient regulatory-protein family of WD-repeat proteins. Nature 371:297–300. doi.org

Nguyen NH, Jung C, Cheong JJ (2019) Chromatin remodeling for the transcription of type 2C protein phosphatase genes in response to salt stress. Plant PhysiolBiochem 141:325–331. doi.org

Papadopoulos JS, Agarwala R (2007) COBALT: constraint-based alignment tool for multiple protein sequences. Bioinformatics (Oxford, England) 23 (9):1073-1079. doi:10.1093/bioinformatics/btm076

Patro R, et al (2017) Salmon provides fast and bias-aware quantification of transcript expression. Nat Methods 14:417–419. doi.org

Peirats-Llobet M, et al (2016) A direct link between abscisic acid sensing and the chromatin-remodeling ATPase BRAHMA via core ABA signaling pathway components. Mol Plant 9:136–147. doi.org

Pratas MI, et al (2018) Inferences on specificity recognition at the *Malus*×*domestica* gametophytic self-incompatibility system. Sci Rep 8:1717. doi.org

Putnam AA, Jankowsky E (2013) DEAD-box helicases as integrators of RNA, nucleotide and protein binding. BiochimBiophys Acta 1829:884–893. doi.org

Rahman S, et al (2011) The Brd4 extraterminal domain confers transcription activation independent of pTEFb by recruiting multiple proteins, including NSD3. Mol Cell Biol 31:2641–2652. doi.org

Reeves R, Beckerbauer L (2001) HMGI/Y proteins: flexible regulators of transcription and chromatin structure. BiochimBiophys Acta 1519:13–29. doi.org

Sakamoto T, et al (2018) Proteasomal degradation of BRAHMA promotes Boron tolerance in Arabidopsis. Nat Commun 9:5285. doi.org

Sanchez R, Zhou MM (2011) The PHD finger: a versatile epigenome reader. Trends Biochem Sci 36:364–372. doi.org

Schindler U, Beckmann H, Cashmore AR (1993) HAT3.1, a novel Arabidopsis homeodomain protein containing a conserved cysteine-rich region. Plant J 4:137–150. doi.org

Schnell JD, Hicke L (2003) Non-traditional functions of ubiquitin and ubiquitin-binding proteins. J Biol Chem 278:35857–35860. doi.org

Soubrier J, Steel M, Lee MSY, Der Sarkissian C, Guindon S, Ho SYW, Cooper A (2012) The Influence of Rate Heterogeneity among Sites on the Time Dependence of Molecular Rates. Molecular Biology and Evolution 29 (11):3345-3358. doi:10.1093/molbev/mss140

Stirnimann CU, et al (2010) WD40 proteins propel cellular networks. Trends Biochem Sci 35:565–574. doi.org

Tamkun JW, et al (1992) Brahma: A regulator of Drosophila homeotic genes structurally related to the yeast transcriptional activator SNF2SWI2. Cell 68:561–572. doi.org

Taunton J, Hassig CA, Schreiber SL (1996) A mammalian histone deacetylase related to the yeast transcriptional regulator Rpd3p. Science 272:408–411. doi.org

Trifinopoulos J, Nguyen LT, von Haeseler A, Minh BQ (2016) W-IQ-TREE: a fast online phylogenetic tool for maximum likelihood analysis. Nucleic Acids Res 44 (W1):W232-235. doi:10.1093/nar/gkw256

Valentinuzzi F, et al (2019) Common and specific responses to iron and phosphorus deficiencies in roots of apple tree (Malus × domestica). Plant Mol Biol 101:129–148. doi.org

Velasco R, et al (2010) The genome of the domesticated apple (*Malus* × *domestica* Borkh.). Nat Genet 42:833–839. doi.org

Waite JM, et al (2023) Transcriptomic approach to uncover dynamic events in the development of mid-season sunburn in apple fruit. G3 (Bethesda) 13:jkad127. doi.org

Waskom M (2021) Seaborn: statistical data visualization. J Open Source Softw 6:3021. doi.org

Wu MF, et al (2012) SWI2/SNF2 chromatin remodeling ATPases overcome polycomb repression and control floral organ identity with the LEAFY and SEPALLATA3 transcription factors. Proc Natl Acad Sci USA 109:3576–3581. doi.org

Yuan D, et al (2014) AtMMS21 regulates DNA damage response and homologous recombination repair in Arabidopsis. DNA Repair 21:140–147. doi.org

Zeng L, et al (2010) Mechanism and regulation of acetylated histone binding by the tandem PHD finger of DPF3b. Nature 466:258–262. doi.org

Zhang C, et al (2023) Gibberellin signaling modulates flowering via the DELLA–BRAHMA–NF-YC module in Arabidopsis. Plant Cell 35:3470–3484. doi.org

Zhang P, et al (2025) Salicylic acid and jasmonic acid in plant immunity. Hortic Res 12:uhaf082. doi.org

Zhao M, et al (2015) Arabidopsis BREVIPEDICELLUS interacts with the SWI2/SNF2 chromatin remodeling ATPase BRAHMA to regulate KNAT2 and KNAT6 expression in control of inflorescence architecture. PLoS Genet 11:e1005125. doi.org

Zhu L, et al (2017) Transcriptomics Analysis of Apple Leaves in Response to *Alternaria alternata* Apple Pathotype Infection. FrontPlantSci 8:22. doi.org